Journal of the Electrochemical Society

The Electrochemical Society
Advancing solid state & electrochemical science & technology

OPEN ACCESS

Simple Way of Making Free-Standing Battery Electrodes and their Use in Enabling Half-Cell Impedance Measurements via μ-Reference Electrode

To cite this article: Robert Morasch *et al* 2020 *J. Electrochem. Soc.* **167** 100540

View the article online for updates and enhancements.

Discover the EL-CELL potentiostats

- Fully independent test channels with Pstat / GStat / EIS
- Optionally with integrated temperature controlled cell chamber
- Unique Connection Matrix: Switch between full-cell and half-cell control at runtime

www.el-cell.com +49 (0) 40 79012 734 sales@el-cell.com

EL-CELL®
electrochemical test equipment

This content was downloaded from IP address 129.187.254.46 on 03/02/2021 at 13:14

Journal of The Electrochemical Society, 2020 **167** 100540

Simple Way of Making Free-Standing Battery Electrodes and their Use in Enabling Half-Cell Impedance Measurements via μ-Reference Electrode

Robert Morasch,[z] Bharatkumar Suthar,[*,a] and Hubert A. Gasteiger[**]

Chair of Technical Electrochemistry, Department of Chemistry and Catalysis Research Center, Technical University of Munich, Munich, Germany

Free-standing electrodes can be useful for a plethora of diagnostic measurements, as they allow transmissive measurements, stacking of electrodes, and/or measurements where the current collector would be disturbing the signal. Another advantage displayed in this publication is their use in Li-ion battery half-cells to decrease and stabilize the impedance of the counter electrode that is usually made of metallic lithium, allowing to conduct electrochemical impedance spectroscopy of a battery-type working electrode via μ-reference electrode which would otherwise show artefacts over a wide range of frequencies. Using measurements on an equivalent circuit mimicking a Li-ion battery half-cell with a μ-reference electrode we show how such artefacts arise from the large resistance in the μ-reference electrode and the imbalance in working and counter electrode resistance. We also show how the use of a free-standing graphite electrode attached to the Li-metal counter electrode (Li/FSG) reduces the counter electrode resistance and allows an artefact-free impedance measurement of the working electrode via a μ-reference electrode. Finally, we show the stability of the Li/FSG electrode and compare it to a Li-metal electrode.
© 2020 The Author(s). Published on behalf of The Electrochemical Society by IOP Publishing Limited. This is an open access article distributed under the terms of the Creative Commons Attribution Non-Commercial No Derivatives 4.0 License (CC BY-NC-ND, http://creativecommons.org/licenses/by-nc-nd/4.0/), which permits non-commercial reuse, distribution, and reproduction in any medium, provided the original work is not changed in any way and is properly cited. For permission for commercial reuse, please email: permissions@ioppublishing.org. [DOI: 10.1149/1945-7111/ab9b93]

Manuscript submitted March 24, 2020; revised manuscript received May 11, 2020. Published June 19, 2020.

The choice of battery cell configuration is important when evaluating the electrochemical properties of anode or cathode active materials with conventional electrolytes or with novel electrolytes/additives for lithium-ion batteries. A convenient initial evaluation can be done using a so-called half-cell configuration with a metallic lithium (Li-metal) counter electrode (CE), providing direct information on the electrochemical properties of the working electrode (WE) active material while, at least ideally, minimizing the influence of the counter electrode on the active material under investigation. A drawback of this approach is that it complicates the analysis of electrochemical impedance spectroscopy (EIS) data, since the Li-metal CE surface morphology/area and, consequently, its impedance varies substantially over the course of cycling (particularly over the first few cycles) as well as over time when no current is applied.[1–3] Therefore, the cell impedance evolution obtained from half-cell measurements with a Li-metal CE does not allow for a rigorous determination of the working electrode impedance, as the impedance of the Li-metal CE cannot be reliably subtracted from the cell impedance. This can only be done by either assembling so-called symmetric cells[4–7] (i.e., cells built with nominally identical electrodes obtained after having subjected them to different charge/discharge procedures) or by making use of a micro-reference electrode (μ-RE). While the former approach requires the experimentally cumbersome harvesting of cycled electrodes and their reassembly in symmetric cells, EIS measurements with μ-REs are non-invasive and more convenient.

In our recent work, Solchenbach et al. had demonstrated the use of a gold wire μ-RE (GWRE)[8] with which one can monitor the impedance evolution of each individual electrode in a full-cell;[8–10] however, so far we could not obtain artefact-free WE impedance spectra with the GWRE technique in a half-cell configuration with a Li-metal CE. As we will show here, this is related to the high impedance of μ-REs (on account of their small cross sectional area), which can result in measurement artefacts. Gómez-Cámer et al.[11] already demonstrated that artefacts can arise when using reference electrodes with high impedance and suggested that activation overpotentials play a role in successfully using a reference electrode for EIS measurements. In the case of battery full-cells consisting of NCM ($LiNi_aCo_bMn_cO_2$, with $a+b+c = 1$) and graphite, Raijmakers et al.,[12] also showed that due to the interplay of the μ-RE impedance and internal impedances of the potentiostat, artefacts can occur at high frequencies (in the kHz regime). Studies done by other groups suggest additional artefacts caused by improper reference electrode positioning, which can produce inhomogeneities in current or potential response.[13–15] A review for Li-ion battery reference electrodes can be found in Ref. 16.

Table I summarizes the above-mentioned advantages and disadvantages of using symmetric cells and -μ-RE for EIS.

In this publication we investigated the source of error for artefacts in EIS measurements via a μ-RE when using a Li-metal counter electrode and developed a method that allows artefact-free EIS measurements of the WE via a μ-RE in a half-cell configuration (i.e., with a working electrode and a Li-metal counter electrode).

We will show that impedance spectra obtained with a μ-reference electrode in a half-cell configuration can show artefacts over a broad frequency range (kHz to mHz). In order to investigate their origin, we conducted comparative EIS measurements on model equivalent circuits composed of a set of actual resistors and capacitors that mimic the half-cell resistor and capacitor elements, but in the absence of any electrochemical reactions. EIS analysis of these model equivalent circuits shows that similar artefacts in the low-frequency region of the impedance spectra occur as observed for actual half-cell impedance spectra, indicating that these artefacts arise from an interplay of potentiostat impedances and cell impedances, whereby the former are generally unknown to the user. Based on the model equivalent circuit measurements, these low-frequency artefacts in half-cells with a Li-metal CE could be eliminated if one were able to substantially decrease the Li-metal impedance. We will show that this can be accomplished experimentally by inserting a free-standing graphite electrode (FSG) between the Li-metal CE and the separator, which establishes a low-impedance counter electrode at a stable Li-metal potential (referred to as Li/FSG). This allows for the acquisition of working electrode impedance spectra that are free of low-frequency artefacts in a cell configuration that essentially represents that of a half-cell with a Li-metal counter electrode.

*Electrochemical Society Member.
**Electrochemical Society Fellow.
[a]Present address: Department of Chemical Engineering, Indian Institute of Technology Bombay, Mumbai 400076, India.
[z]E-mail: robert.morasch@tum.de

Table I. Overview of the cardinal advantages and disadvantages of electrochemical impedance measurements via symmetric cells and cells with a μ-RE (WE = working electrode; CE = counter electrode).

	Advantages	Disadvantages
symmetric cell	impedance determination of anode or cathode	requires electrode harvesting
μ-RE	operando impedance meas. of individual electrodes	measurement artefacts when using a Li-metal CE
μ-RE with modified Li-metal CE (this publication)	artefact-free measurements of the WE via the μ-RE	requires additional assembly step

Experimental

Preparation of free-standing electrodes.—The following describes an easy approach to produce free-standing PVDF-bonded electrodes. Other methods to produce free-standing electrodes can be found elsewhere.[17,18] The two here proposed methods (acc. to procedures A or B, see Fig. 1) are suitable to produce free-standing PVDF-bonded electrodes of both graphite and NCM (or other cathode active materials), whereby for the latter only procedure A can be used, as electrodes with cathode active materials generally should not be immersed in water. The first step in preparing free-standing electrodes is coating a thin layer of sodium carboxymethyl cellulose (CMC, Sigma Aldrich) binder onto a current collector foil. The CMC binder was mixed at a CMC to H_2O ratio of 1:25 (wt:wt) and coated at a wet film thickness of 30 μm onto a copper current collector foil (MTI, 12 μm) attached to a glass plate using a gap bar coater (RK PrintCoat Instruments, UK). To prepare a free-standing graphite electrode, graphite (T311 type from SGL, with 19 μm D50 and 3 $m^2\,g^{-1}$) and polymer binder (polyvinylidene fluoride (PVDF), Arkema) at a ratio of 95:5 (wt:wt) were mixed with N-Methyl-2-pyrrolidone (NMP, Sigma Aldrich, anhydrous, 99.5%) at a solid to liquid ratio of 5:4 (wt:wt) in a planetary mixer (Thinky ARV-310) at 2000 rpm for five minutes. The prepared graphite slurries were coated onto the CMC-coated copper current collector at a wet film thickness of 200 μm. Free-standing cathode electrodes can be prepared analogously.

Since the CMC layer is not soluble in NMP, it serves to block the PVDF binder of the electrode coated on top of it from adhering to the current collector foil. The dried electrode is then put into a bath of ethanol (see panel A1 in Fig. 1, left-hand-side) or water (see panel B1 in Fig. 1, right-hand-side), whereby the latter is only recommended for materials stable in H_2O. Since CMC is not soluble in ethanol, the CMC film is not dissolved, but its surface becomes non-adherent and the electrode can be peeled or swiped off the surface with little effort (see panels A1-3 in Fig. 1). For graphite electrodes, the electrode sheet can also be immersed in a water bath in which the CMC layer dissolves, leaving the electrode detached from the surface, which can also easily be done with already punched electrodes (see panels B1-3 in Fig. 1). As CMC is commonly used in battery electrodes, residual CMC in the electrode is of little concern in battery tests; however, if necessary, it could be removed in an additional washing step. Additionally heating the water bath is possible to speed up the dissolution process of the CMC but no heat treatment was performed for this work. For the free-standing graphite (FSG) electrodes used in this study, only procedure A was used.

The thickness of the here prepared dried and uncompressed free-standing graphite electrodes and of conventional graphite working electrodes (prepared as above, but without the CMC interlayer) was ~105 μm (±2%), corresponding to graphite loadings of ~9.8 mg cm^{-2} (±2%) with an areal capacity of ~3.4 mAh cm^{-2} (calculated for a theoretical graphite capacity of 350 mAh g^{-1}). The electrodes were not further compressed/calendered, and their porosity was ~55% (based on thickness and areal weight measurements). The dried electrodes were punched out to a diameter of 10.95 mm (equating to an area of ~0.94 cm^2) using an electrode punch (Hohsen Corp. OSAKA, Japan). Alternatively, a carbon paper (5% hydrophobized ~360 μm thick Toray carbon fiber paper T120, Toray) was used as free-standing electrode and applied as received. The Carbon paper has a roughness factor of ~18 $cm^2_{BET}\,cm^{-2}$, based on ~7 $mg_{carbon}\,cm^{-2}$ areal weight and ~0.25 $m^2\,g^{-1}$ BET area while the FSG electrode has a roughness factor of ~300 $cm^2_{BET}\,cm^{-2}$, based on ~9.8 $mg_{graphite}\,cm^{-2}$ areal weight and ~3 $m^2\,g^{-1}$ BET area.

Equivalent circuit.—The equivalent circuit for the impedance measurements shown in Fig. 2b was soldered according to the circuit description of Fig. 2a, using carbon film resistors (Conrad Electronic GmbH, Germany) and electrolyte (⩾1 μF) or film (1 nF) capacitors (Conrad Electronic GmbH, Germany).

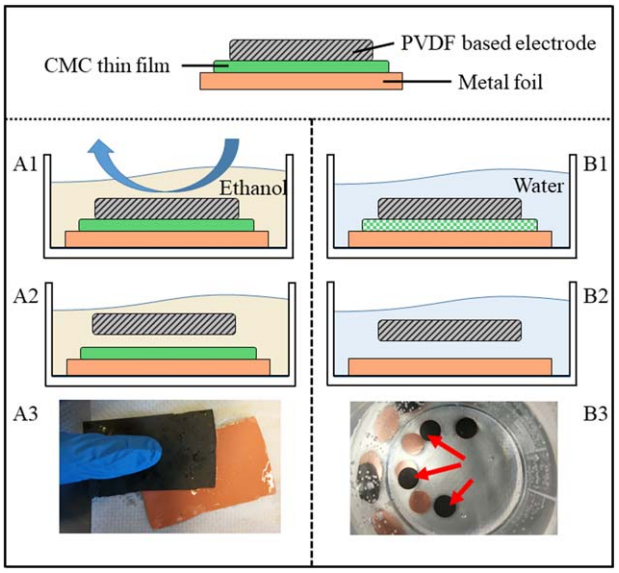

Figure 1. Depiction of the free-standing electrode preparation process based on a current collector foil (here copper foil) coated with a CMC layer onto which subsequently a PVDF-bonded electrode is coated (here graphite). Process A (left-hand-side): Immersion of the copper/CMC/graphite assembly into ethanol (A1), which causes a loss of adhesion between the graphite electrode and the CMC film, without dissolving the CMC film (A2). The electrode can then be swiped off the current collector with little effort, shown in panel A3 for a graphite electrode. Process B (right-hand-side): Alternatively, the electrode can be immersed in water (B1) to dissolve the CMC film, leading to the detachment of the electrode (B2), as seen in panel B3 for graphite electrodes punched at 10.95 mm diameter (red arrows indicate detached electrodes).

Cell assembly, charge/discharge cycling, and impedance measurement.—For electrochemical impedance analysis, a three-electrode cell setup (Swagelok® T-cell) with a gold-wire reference electrode (GWRE, described in more detail in Fig. 1b in Ref. 8) was used. The cells were built inside an argon filled glove box (MBraun, 25 °C ± 1 °C, oxygen and water content <0.1 ppm, Ar 5.0, Westfalen). All cell parts were dried at 120 °C in a vacuum oven (Büchi, Switzerland) for 8 h before being transferred into an Ar-filled glovebox.

The cells were assembled with a graphite working electrode (areal capacity ~3.4 mAh cm^{-2}), two porous glass fiber separators with a diameter of 11 mm (VWR, 250 μm uncompressed thickness, 90% porosity), and a counter electrode consisting of either a metallic lithium foil (0.45 mm thickness and 11 mm diameter, Rockwood Lithium) or a free-standing graphite electrode firmly attached to the metallic lithium foil (referred to as Li/FSG). For cycling stability tests and impedance analysis of the Li-metal or the Li/FSG electrodes, symmetric cells in a three-electrode cell setup as described above were assembled. 80 μl of LP57 electrolyte (1 M $LiPF_6$ in EC:EMC 3:7 (wt:wt), battery grade, BASF) were added to the cells. Using a potentiostat (Bio-Logic Science Instruments, France), the gold-wire reference electrode was lithiated at 150 nA for 1 h via the Li-metal or Li/FSG counter electrode in a temperature-controlled chamber (25 °C, Binder).

The cycling protocol started with a 3 h open circuit voltage phase to allow for complete wetting of the electrodes and stabilization of the Li/FSG counter electrode. Lithiation of the graphite working electrode was performed galvanostatically (constant current lithiation) at C/10 to 40 mV vs Li^+/Li without prior formation. Potentiostatic electrochemical impedance measurements over the course of cycling were performed at open circuit voltage (OCV) at

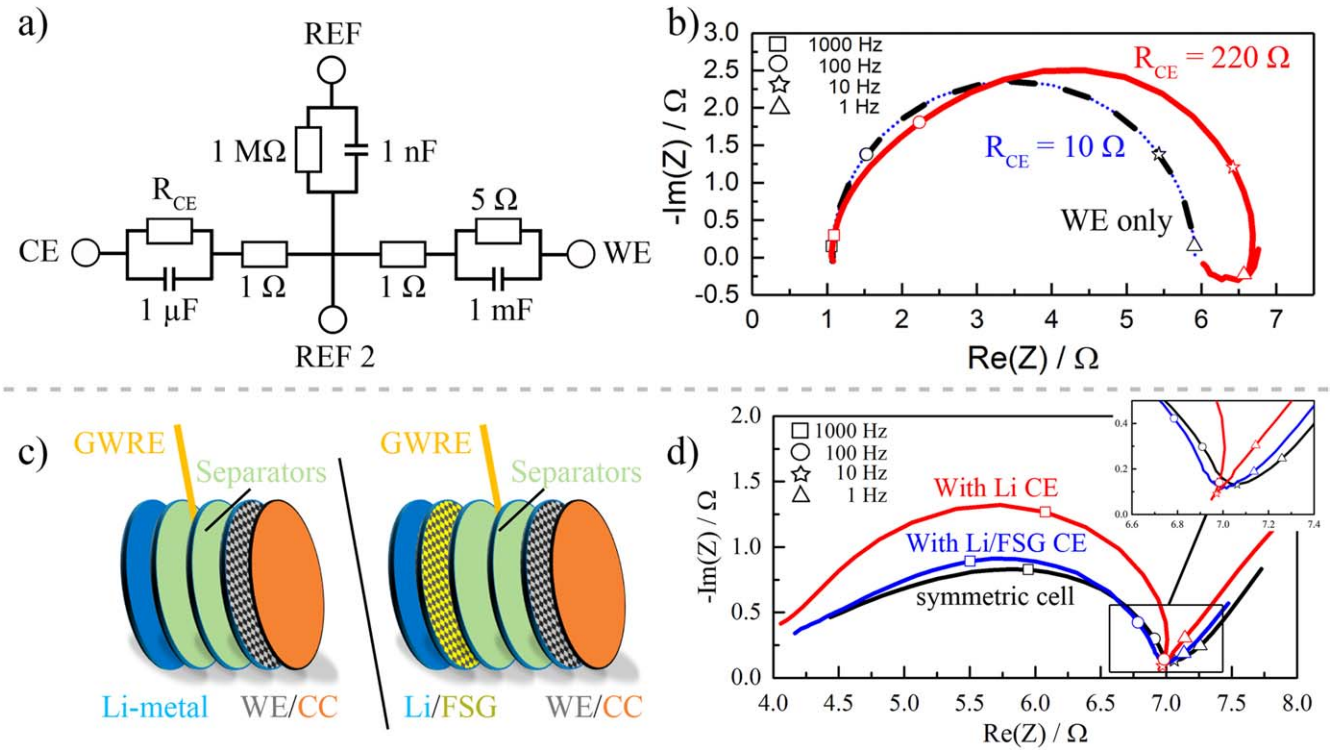

Figure 2. Comparison of the working electrode impedance (30 kHz to 0.1 Hz) of model equivalent circuits and of the graphite working electrode (at 100% SOC) in half-cells with a GWRE and with different counter electrodes. (a) Model equivalent circuit mimicking a lithium-ion battery half-cell with a gold-wire μ-RE with the indicated resistance and capacitance values (for choice of values see text), using a CE resistance (R_{CE}) of either 220 Ω or 10 Ω. (b) Impedance response of the WE of the model equivalent circuit with R_{CE} = 220 Ω (red) or R_{CE} = 10 Ω (dotted blue line), and comparison of the impedance responses to that of the individually measured WE (dashed black line; perfectly overlapping with the dotted blue line), where the RE and CE cables of the potentiostat are not connected to contacts CE and REF, respectively but are instead both connected to the contact marked as REF 2 in Fig. 2a). (c) Half-cell configuration with a graphite electrode (gray), a GWRE (yellow line) sandwiched between two separators (green), and either a Li-metal CE (blue; left sketch) or a Li-metal CE with an attached FSG electrode (yellow; right sketch). (d) Impedance response of the graphite WE obtained by either one of the two configurations shown in (c), i.e., either with a Li-metal CE (Li-CE, red line) or with an Li/FSG CE (blue line). For comparison, the black line shows the impedance response of the graphite WE in a symmetric cell (overall cell impedance divided by two).

100% state-of-charge (SOC) from 30 kHz to 0.1 Hz and with an excitation of 10 mV. For symmetric cell measurements, graphite electrodes prepared as mentioned above were charged to 40 mV, harvested, rinsed three times with 0.1 ml of diethylene carbonate (BASF SE, Germany), and re-assembled into symmetric cells using the above described assembly protocol but without a GWRE.

Results and Discussion

Impedance artefacts observed with model equivalent circuits.— There are multiple sources of error for impedance measurements, ranging from the potentiostat to artefacts that may arise from an individual cell design or cell chemistry.[11–15] To exclude any source of artefacts that may be caused by the three-electrode T-cell setup or from electrochemical phenomena in the half-cell, the cell setup was mimicked as a model equivalent circuit using actual resistors and capacitors, allowing us to probe whether the potentiostat controls circuitry might lead to impedance artefacts.

Figure 2a shows the simplified equivalent circuit that represents a lithium-ion battery half-cell with a gold wire μ-reference electrode. Each of the three electrodes is represented by a parallel resistor/capacitor element (further on referred to as R/C element) with approximate resistance and capacitance values that represent those of a lithium-ion battery half-cell composed of a μ-RE, a Li-metal CE, a conventional graphite WE, and a separator:

(1) The resistance and capacitance of the here used μ-RE (the GWRE) were measured to be on the order of 10^6 Ω and 1 nF, respectively, values which were used in the REF-branch of the model equivalent circuit (see top branch in Fig. 2a) and which can be rationalized by the very small GWRE cross sectional area of $\sim 20 \times 10^{-6}$ cm^2 (this equates to a reasonable GWRE charge transfer resistance of 20 Ω·cm^2).

(2) The Li-metal CE resistance was measured to be on the order of 10^2 Ω (based on Li/Li symmetric cell measurements, see Fig. 3a, red and green lines) and its capacitance was measured to be on the order of 1 μF (calculated from the semicircle apex at 1077 Hz of the Li-metal impedance response, red line Fig. 3a); both values are consistent with previous measurements.[8] Thus, the capacitance for the Li-metal CE part of the model equivalent circuit (left branch in Fig. 2a) was set to 1 μF, while its resistance was set to R_{CE} = 220 Ω. However, in order to investigate the effect of a lower CE resistance on the impedance response of the model equivalent circuit, we also conducted experiments with a resistor of R_{CE} = 10 Ω.

(3) The graphite working electrode resistance was approximated to be on the order of 5 Ω (see right branch in Fig. 2a), based on previous measurements with the same graphite material which showed overall graphite anode low-frequency resistances of ~2-4 Ω[8,10] for ~1.5-fold lower loadings. The capacitance was set to 1 mF, representing the large surface area of a standard battery electrode (the frequency of the data point closest to the apex in Fig. 2b [dashed black and dotted blue line] is 35 Hz).

(4) Finally, the commonly observed overall resistance for the separator of ~2 Ω[10] was divided into two 1 Ω resistances (see center part of the circuit in Fig. 2a).

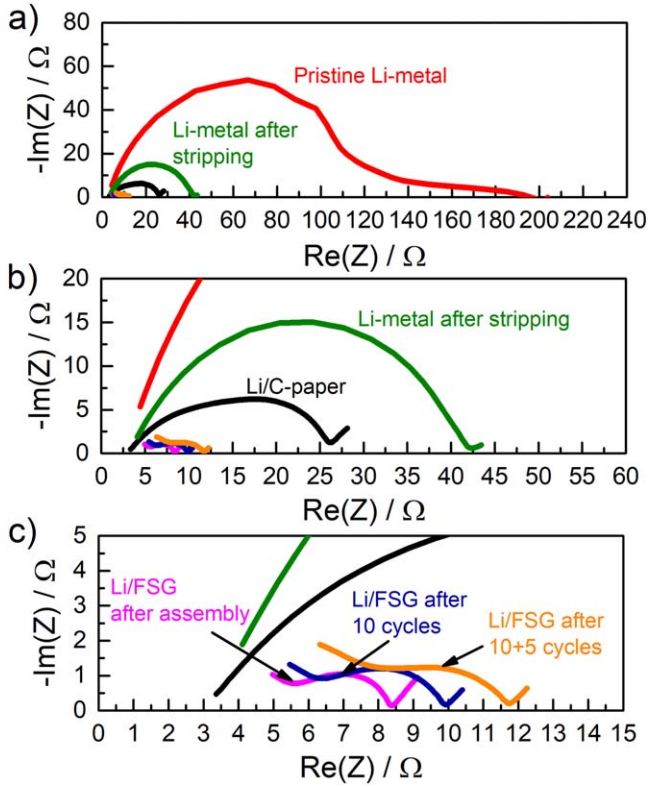

Figure 3. Nyquist plots at different levels of magnification, showing the WE impedance response obtained by means of a μ-RE in symmetric Li//Li, Li/FSG//Li/FSG, or Li/C-paper//Li/C-paper cells. (a) Impedance response of a pristine Li-metal WE, measured ~3 h after assembly, with a low-frequency resistance (LFR) of ~200 Ω (red lines). After Li-stripping at 0.32 mA cm^{-2}, the Li-metal LFR is significantly reduced to ~40 Ω (green lines). (b) Zoom of(a), illustrating the lowering of the LFR to ~25 Ω (corrected by the HFR) when a carbon fiber paper is attached to the Li-metal (Li/C-paper; black lines), measured ~3 h after assembly. (c) Zoom of (b), depicting the impedance response of the Li/FSG WE measured ~3 h after assembly (magenta lines) and showing an LFR of ~3–4 Ω (corrected for the HFR and $R_{contact}$); the LFR of the Li/FSG WE increases gradually after 10 cycles with 10 h of Li-stripping and Li-plating at ±0.21 mA cm^{-2} (blue lines), and after 5 additional cycles at ±0.42 mA cm^{-2} (orange lines).

The model equivalent circuit (Fig. 2a) was measured with two different resistance values for the counter electrode, namely with $R_{CE} = 220\ \Omega$ to represent the typical value of a Li-metal CE (see above), and with a substantially lower value of $R_{CE} = 10\ \Omega$. Figure 2b shows the resulting Nyquist plots for the WE impedance measured via the reference electrode terminal (i.e., the RE cable of the potentiostat is connected to the contact marked REF in Fig. 2a; WE and CE cables are connected to the contacts marked WE and CE, respectively). For $R_{CE} = 220\ \Omega$ (red line), the WE impedance response (red line in Fig. 2b) shows an "overshoot" for frequencies below 110 Hz if compared to the expected semi-circle shape obtained when directly measuring the R/C circuit representing the working electrode (dashed black line; here, the RE and CE cables of the potentiostat are connected both to the contact marked REF 2 in Fig. 2a). Furthermore, a non-physical "back-looping" of the low-frequency branch is observed towards the lowest measured frequencies (i.e., near 0.1 Hz; see red line). Surprisingly, lowering the CE resistance to $R_{CE} = 10\ \Omega$ gives the correct response of the impedance measurement (compare dotted blue and dashed black line). This is unexpected, as the magnitude of the counter electrode impedance should not influence the impedance response of the WE measured via a reference electrode. The exact reason for this artefact is not known, but we presume this to be an effect caused by the large impedance of the reference electrode in combination with the unknown internal impedances of the potentiostat, similarly to the descriptions in Ref. 12 Other explanations for the existence of impedance artefacts relating to the cell geometry and the reference electrode location[12–15] can be excluded, as the measurement on the model equivalent circuit is not affected by such influences. Hence, the correct impedance response with a high impedance μ-RE can be obtained by decreasing the value of the CE resistance, so that it is of a similar order of magnitude as that of the WE.

Graphite working electrode impedances in half-cells using a μ-RE.—The following section describes an approach to minimize and stabilize the impedance response of the Li-metal CE in order to allow for artefact-free EIS measurements of the WE using a μ-RE in a half-cell setup.

The impedance artefacts observed with the model equivalent circuit explain why artefact-free impedances can be obtained in full-cells with a μ-RE,[8–10] as there the WE and the CE have comparable impedances. On the other hand, it also explains why we so far had not been able to acquire artefact-free WE impedances in half-cells with a Li-metal CE, as there the impedance of the WE is typically 10^1-10^2 times larger than that of the CE (see estimates above). The latter is illustrated by the graphite WE impedance response obtained for a half-cell with a GWRE and with a Li-metal CE (red line in Fig. 2d; cell configuration shown in the left panel of Fig. 2c), where a back-looping of the Nyquist plot near the low-frequency region occurs, rather similar to what was observed for the model equivalent circuit when $R_{CE} \gg R_{WE}$ (red line in Fig. 2b).

As mentioned in the introduction, half-cell measurements with a Li-metal CE provide valuable insights when evaluating new/modified anode or cathode active materials as working electrode, since the effect of a loss of cyclable lithium can be avoided by the large lithium excess and since the CE potential is well-defined (at least at low current densities, i.e., at low charge/discharge rates). However, in order to also enable an evaluation of the WE impedance with a μ-RE (i.e., in-situ, without the need to reassemble symmetric cells), the impedance of the Li-metal CE would need to be substantially reduced. This can be achieved by attaching a free-standing graphite electrode to the Li-metal surface, according to the cell configuration shown in the right-hand panel of Fig. 2c. Once the cell is filled with electrolyte, the free-standing graphite in contact with the metallic lithium (Li/FSG) is immediately lithiated and reaches a stable potential of 0 V vs Li^+/Li within ~3 h. At the same time, the largely increased interfacial surface area of the Li/FSG vs. the Li-metal CE leads to a drastic reduction of the CE impedance (as will be shown below), which should enable the acquisition of artefact-free WE impedances in a half-cell with a μ-RE and an Li/FSG CE. That this is indeed the case is shown by the graphite WE impedance response when using a GWRE and a low-impedance Li/FSG CE, and by comparing it to the symmetric cell measurement (blue and black line in Fig. 2d), where the back-looping of the Nyquist plot near the low-frequency region does not anymore appear, as expected on the basis of the model equivalent circuit experiments (blue line in Fig. 2b). This demonstrates that artefact-free in-situ WE impedance data can be obtained in a half-cell configuration, when a FSG is attached to a conventional Li-metal CE to lower its impedance. The apex frequency values of the measured graphite impedances for all three measurements in Fig. 2d (around 1 kHz) are more than one order of magnitude higher than the apex of the equivalent circuit measurements in Fig. 2b (around 35 Hz). This is the result of the more complex impedance of the graphite electrode which does not only include the charge transfer resistance, but also the pore resistances from the electrolyte within the pores of the graphite electrode as well as the solid electrolyte interphase. A detailed analysis of the graphite impedance will be shown in a later publication. In a recent work, we had also shown that the free-standing electrode concept can equally well be applied to determine the working electrode impedance in sodium-ion battery half-cells, using carbon paper attached to metallic sodium as the counter electrode.[19]

Impedances of Li-metal, Li/FSG, and Li/C-paper electrodes.— As the resistance of the CE is an important factor in enabling artefact-free EIS measurements of the WE via a μ-RE, we compared three different CE designs in order to give an overview over the range of resistance for different electrode designs: (i) lithium metal (referred to as Li-metal), (ii) carbon paper attached to Li-metal (referred to as Li/C-paper), and (iii) a FSG electrode attached to Li-metal (referred to as Li/FSG).

In order to obtain estimates for the impedance of a Li-metal electrode, a Li/FSG electrode, and a Li/C-paper, symmetric cells (i.e., Li//Li, Li/FSG//Li/FSG, and Li/C-paper//Li/C-paper cells) equipped with a GWRE were assembled. The impedance response (potentiostatic at OCV) of the working electrode (i.e., one of the two electrodes in the cell) was recorded using the GWRE. As shown in Fig. 3a, the low-frequency resistance (LFR, corrected by the high-frequency resistance (HFR)) of the pristine Li-metal electrode is $\sim$200 Ω (red lines) and gets reduced substantially to $\sim$40 Ω (green lines) after 5 h of Li-stripping at 0.32 mA cm^{-2} (for the graphite WE used in this study, this would correspond to a C-rate of $\sim$0.1 h^{-1}). We attribute the drastic change in the lithium metal impedance to the change in lithium surface area after stripping, highlighting why cell impedance measurements of half-cells with a Li-metal CE and without a reference electrode do not allow to quantify the impedance of the WE. Figure 3b shows the impedance response of a Li/C-paper electrode (black line), which is a quick and easy alternative to a free-standing graphite electrode, as it is commercially available and can be applied as-received. While its LFR is lower than that of Li-metal ($\sim$25 Ω), it is still $\sim$7 times larger compared to that of the pristine Li/FSG electrode ($\sim$3–4 Ω; see magenta lines in Fig. 3c), in part due to the roughly one order of magnitude smaller surface area of the C-paper (see experimental section).

Owing to the very low impedance of the Li/FSG electrode, the presence of a contact resistance ($R_{contact}$) can be discerned at high frequencies, which must be due to an imperfect lamination between the FSG and the Li-metal, so that the LFR for the Li/FSG electrode contains contributions from this contact resistance. Nevertheless, the overall LFR of the Li/FSG electrode is roughly an order of magnitude lower than that of Li-metal and rather similar to the LFR of a conventional graphite electrode ($\sim$8 Ω, see black line in Fig. 2d).

In order to evaluate the variation of the Li/FSG electrode impedance with cycling, the Li/FSG//Li/FSG cell was additionally cycled 10 times at $\pm$0.21 mA cm^{-2} for 10 h (10 h stripping and 10 h plating per cycle). The blue line in Fig. 3c shows the impedance response after 10 cycles. The electrode impedance is slightly larger, with an additional shift to higher values attributed to an increase in electrical contact resistance between the FSG and the Li-metal (this could likely be suppressed by a higher cell compression, which in the current experiments is $\sim$2 bar, set by a spring).[8] After 5 additional cycles at $\pm$0.42 mA cm^{-2} for 5 h (i.e., 5 h stripping and 5 h plating per cycle), the impedance again shifts to the right, attributed to an additional increase in contact resistance. Overall, the Li/FSG electrode shows a slow increase in impedance for low current cycling; its impedance is independent of the state-of-charge of the working electrode, since on account of the quasi unlimited Li-supply from the Li-metal, the Li/FSG potential remains at 0 V vs Li^{+}/Li at OCV, where the impedance data are acquired. In this configuration, the WE impedance can in principle be estimated even from *cell* impedances acquired for half-cells with an Li/FSG CE and without a μ-RE over the course of a few cycles, if the impedance response of the Li/FSG electrode was measured independently beforehand, e.g., in symmetric cells. In this case, any reversibly measured changes in *cell* impedance can be attributed to changes of the working electrode impedance, allowing the user to extract useful information from a half-cell impedance measurement even without reference electrode. Such a setup was not used in this publication and it is of the discretion of the individual reader to determine its validity for individual setups.

Choosing the proper type of free-standing electrode.—As shown in this publication, the choice of CE affects the ability to perform artefact-free impedance analysis of the WE via a μ-RE. Two options of free-standing electrode to minimize the CE impedance and to enable the measurement of the WE impedance were presented here. First, the free-standing graphite electrode (FSG) attached to a Li-metal electrode (Li/FSG) shows the lowest impedance and is therefore best suited to allow the use of a μ-RE for any commercial Li-ion battery active materials known to the authors. This is true for a free-standing electrode of a reasonable loading of 1–3 mAh cm^{-2} comprised of commercially available graphite for Li-ion batteries. Its drawback, however, are the additional steps needed to produce the electrode and during cell assembly.

Using a carbon paper in contact with Li-metal (Li/C-paper) is more convenient, as carbon papers are commercially available and can be used as received. The drawback of the Li/C-paper configuration is its generally higher impedance (depending on the type of carbon paper), which is why it may not be suited for measurements of all types of working electrodes.

In all cases, however, the individual user needs to know the resistance range of the working electrode to be examined and should, for best practice, ensure that the counter electrode resistance is always equal or lower in resistance compared to the WE as the impedance ratio of WE and CE that marks the onset of artefacts is not know and may depend heavily on the cell setup and potentiostat.

Regarding the choice of Li-metal, any commercially available Li-metal films with thickness of 75 μm and above are sufficiently overbalanced to serve as Li-source for this setup.

Conclusions

This publication shows a simple approach to produce free-standing PVDF-bonded graphite electrodes, which in principle can also be extended to water-sensitive PVDF-bonded cathode active material electrodes.

We show how the use of free-standing graphite (FSG) electrodes attached to a metallic lithium electrode (referred to as Li/FSG) allows to determine the electrochemical impedance response of a battery-type working electrode (WE) in Li-ion battery half-cells equipped with a micro-reference electrode (μ-RE). This approach overcomes the impedance artefacts that are encountered over a wide frequency range when using a half-cell configuration with a conventionally used Li-metal counter electrode (CE), which we show to result from the large impedance difference between a typical Li-ion battery electrode as WE and a Li-metal CE in conjunction with a high-impedance μ-RE. That these artefacts are caused by the potentiostat controls circuitry is demonstrated by impedance measurements on a set of resistors and capacitors the mimick a Li-Ion battery half-cell.

Thus, the use of a Li/FSG counter electrode that is characterized by a very low impedance compared to a Li-metal CE allows for artefact-free measurements of the WE impedance in a half-cell configuration via a μ-reference electrode. The impedance response of the Li/FSG electrodes was found to be reasonably stable for low cycle numbers.

Acknowledgments

R. M. gratefully acknowledges the funding by the BMWI (Federal Ministry for Economic Affairs and Energy, Germany) for its financial support under the auspices of the SurfaLIB project (grant number 03ET6103F). B. S. acknowledges the financial support from the BMBF (Federal Ministry of Education and Research, Germany), under the auspices of the ExZellTUM II project (grant number 03XP0081). We would also like to thank Daniel Pritzl, Fabian Linsenmann, and Johannes Landesfeind for valuable discussions.

ORCID

Robert Morasch https://orcid.org/0000-0002-9931-1022

References

1. D. Aurbach, A. Zaban, A. Schechter, Y. Ein-Eli, E. Zinigrad, and B. Markovsky, *J. Electrochem. Soc.*, **142**, 2873 (1995).
2. A. Zaban, E. Zinigrad, and D. Aurbach, *J. Phys. Chem.*, **100**, 3089 (1996).
3. J. Y. Song, H. H. Lee, Y. Y. Wang, and C. C. Wan, *J. Power Sources*, **111**, 255 (2002).
4. J. C. Burns, L. J. Krause, D. B. Le, L. D. Jensen, A. J. Smith, D. Xiong, and J. R. Dahn, *J. Electrochem. Soc.*, **158**, A1417 (2011).
5. R. Petibon, C. P. Aiken, N. N. Sinha, J. C. Burns, H. Ye, C. M. VanElzen, G. Jain, S. Trussler, and J. R. Dahn, *J. Electrochem. Soc.*, **160**, A117 (2013).
6. N. Ogihara, S. Kawauchi, C. Okuda, Y. Itou, Y. Takeuchi, and Y. Ukyo, *J. Electrochem. Soc.*, **159**, A1034 (2012).
7. C. H. Chen, J. Liu, and K. Amine, *J. Power Sources*, **96**, 321 (2001).
8. S. Solchenbach, D. Pritzl, E. J. Y. Kong, J. Landesfeind, and H. A. Gasteiger, *J. Electrochem. Soc.*, **163**, A2265 (2016).
9. J. Landesfeind, D. Pritzl, and H. A. Gasteiger, *J. Electrochem. Soc.*, **164**, A1773 (2017).
10. D. Pritzl, J. Landesfeind, S. Solchenbach, and H. A. Gasteiger, *J. Electrochem. Soc.*, **165**, A2145 (2018).
11. J. L. Gómez-Cámer and P. Novák, *Electrochem. Commun.*, **34**, 208 (2013).
12. L. H. J. Raijmakers, M. J. G. Lammers, and P. H. L. Notten, *Electrochim. Acta*, **259**, 517 (2018).
13. M. Ender, J. Illig, and E. Ivers-Tiffée, *J. Electrochem. Soc.*, **164**, A71 (2017).
14. J. Costard, M. Ender, M. Weiss, and E. Ivers-Tiffée, *J. Electrochem. Soc.*, **164**, A80 (2017).
15. A. Battistel, M. Fan, J. Stojadinović, and F. La Mantia, *Electrochim. Acta*, **135**, 133 (2014).
16. R. Raccichini, M. Amores, and G. Hinds, *Batteries*, **5**, 1 (2019).
17. I. V. Thorat, D. E. Stephenson, N. A. Zacharias, K. Zaghib, J. N. Harb, and D. R. Wheeler, *J. Power Sources*, **188**, 592 (2009).
18. F. Pouraghajan, H. Knight, M. Wray, B. Mazzeo, R. Subbaraman, J. Christensen, and D. Wheeler, *J. Electrochem. Soc.*, **165**, A2644 (2018).
19. F. Linsenmann, D. Pritzl, and H. A. Gasteiger, *J. Electrochem. Soc.*, **166**, A3668 (2019).